Determination of the pion charge form factor for $Q^2 = 0.60$–1.60 GeV^2

V. Tadevosyan,[1] H. P. Blok,[2,3] G. M. Huber,[4] D. Abbott,[5] H. Anklin,[5,6] C. Armstrong,[7] J. Arrington,[8] K. Assamagan,[9]
S. Avery,[9] O. K. Baker,[5,9] C. Bochna,[10] E. J. Brash,[4] H. Breuer,[11] N. Chant,[11] J. Dunne,[5] T. Eden,[5,12] R. Ent,[5] D. Gaskell,[13]
R. Gilman,[5,14] K. Gustafsson,[11] W. Hinton,[9] H. Jackson,[8] M. K. Jones,[7] C. Keppel,[5,9] P. H. Kim,[15] W. Kim,[15] A. Klein,[16]
D. Koltenuk,[17] M. Liang,[5] G. J. Lolos,[4] A. Lung,[5] D. J. Mack,[5] D. McKee,[18] D. Meekins,[7] J. Mitchell,[5] H. Mkrtchyan,[1]
B. Mueller,[8] G. Niculescu,[9] I. Niculescu,[9] D. Pitz,[19] D. Potterveld,[8] L. M. Qin,[16] J. Reinhold,[8] I. K. Shin,[15] S. Stepanyan,[1]
L. G. Tang,[5,9] R. L. J. van der Meer,[4] K. Vansyoc,[16] D. Van Westrum,[20] J. Volmer,[2,3] W. Vulcan,[5] S. Wood,[5] C. Yan,[5]
W.-X. Zhao,[21] and B. Zihlmann[5,22]

(Jefferson Lab F$_\pi$ Collaboration)

[1]*Yerevan Physics Institute, 375036 Yerevan, Armenia*
[2]*Faculteit Natuur-en Sterrenkunde, Vrije Universiteit, NL-1081 HV Amsterdam, The Netherlands*
[3]*NIKHEF, Postbus 41882, NL-1009 DB Amsterdam, The Netherlands*
[4]*University of Regina, Regina, Saskatchewan S4S-0A2, Canada*
[5]*Physics Division, TJNAF, Newport News, Virginia 23606, USA*
[6]*Florida International University, Miami, Florida 33119, USA*
[7]*College of William and Mary, Williamsburg, Virginia 23187, USA*
[8]*Argonne National Laboratory, Argonne, Illinois 60439, USA*
[9]*Hampton University, Hampton, Virginia 23668, USA*
[10]*University of Illinois, Champaign, Illinois 61801, USA*
[11]*University of Maryland, College Park, Maryland 20742, USA*
[12]*Norfolk State University, Norfolk, Virginia 23504, USA*
[13]*Oregon State University, Corvallis, Oregon 97331, USA*
[14]*Rutgers University, Piscataway, New Jersey 08855, USA*
[15]*Kyungpook National University, Taegu, Korea*
[16]*Old Dominion University, Norfolk, Virginia 23529, USA*
[17]*University of Pennsylvania, Philadelphia, Pennsylvania 19104, USA*
[18]*New Mexico State University, Las Cruces, New Mexico 88003-8001, USA*
[19]*DAPNIA/SPhN, CEA/Saclay, F-91191 Gif-sur-Yvette, France*
[20]*University of Colorado, Boulder, Colorado 76543, USA*
[21]*M.I.T.-Laboratory for Nuclear Sciences and Department of Physics, Cambridge, Massachusetts 02139, USA*
[22]*University of Virginia, Charlottesville, Virginia 22901, USA*

The data analysis for the reaction ^{1}H($e, e'\pi^+$)n, which was used to determine values for the charged pion form factor F_π for values of $Q^2 = 0.6$–1.6 GeV^2, has been repeated with careful inspection of all steps and special attention to systematic uncertainties. Also the method used to extract F_π from the measured longitudinal cross section was critically reconsidered. Final values for the separated longitudinal and transverse cross sections and the extracted values of F_π are presented.

I. INTRODUCTION

Hadron form factors are an important source of information on hadronic structure. Of these, the electric form factor, F_π, of the charged pion plays a special role. One of the reasons is that the valence structure of the pion is relatively simple. The hard part of the π^+ form factor can be calculated within the framework of perturbative QCD (pQCD) as the sum of logarithms of Q^2 multiplied by powers of $1/Q^2$ [1]. As $Q^2 \to \infty$, only the leading-order term remains

$$F_\pi(Q^2 \to \infty) \to \frac{16\pi\alpha_s(Q^2)f_\pi^2}{Q^2}, \qquad (1)$$

where α_s is the strong-coupling constant and f_π the pion decay constant. Thus, in contrast to the nucleon case, the asymptotic normalization of the pion function is known from the decay of

the pion. The theoretical prediction for F_π at experimentally accessible Q^2 is less certain, because the calculation of the soft contributions is difficult and model dependent. This is where considerable theoretical effort has been expended in recent years. Some examples include next-to-leading order (NLO) quantum chromodynamics (QCD) [2,3], QCD sum rules [4,5], constituent quark models [6], and Bethe-Salpeter equation [7] calculations. (See Ref. [8] for a review.) Some of these approaches are more model independent than others, but it is fair to say that all benefit from comparison to high-quality F_π data to delineate the role of hard versus soft contributions at intermediate Q^2.

The experimental measurement of the pion form factor is quite challenging. At low Q^2, F_π can be measured in a model-independent manner via elastic scattering of π^+ from atomic electrons such as at the CERN Super Proton Synchrotron

(SPS) [9]. Above $Q^2 > 0.3$ GeV^2, one must determine F_π from pion electroproduction on the proton. The dependence on F_π enters the cross section via the t-channel process, in which the incident electron scatters from a virtual pion, bringing it on-shell. This process dominates near the pion pole at $t = m_\pi^2$. The physical region for t in pion electroproduction is negative, so measurements should be performed at the smallest attainable values of $-t$. To minimize background contributions, it is also necessary to separate the longitudinal cross section σ_L, via a Rosenbluth L/T(/LT/TT) separation. The value of $F_\pi(Q^2)$ is then determined by comparing the measured longitudinal cross section at small values of $-t$, where it is dominated by the t-pole term, which contains F_π, to the best available model for the reaction ^{1}H$(e, e'\pi^+)n$, adjusting the value of F_π in the latter.

Using the electroproduction technique, the pion form factor was studied for Q^2 values from 0.4 to 9.8 GeV^2 at CEA/Cornell [10] and for $Q^2 = 0.35$ and 0.70 GeV^2 at DESY [11,12]. Reference [12] performed a longitudinal/transverse separation by taking data at two values of the electron energy. In the experiments done at CEA/Cornell, this was done in a few cases only, but even then the resulting uncertainties in σ_L were so large that the L/T separated data were not used, and σ_L was determined by assuming a certain parametrization for σ_T. Consequently, the values of F_π extracted from these data have sizable systematic uncertainties.

More recently, the ^{1}H$(e, e'\pi^+)n$ reaction was measured at the Thomas Jefferson National Accelerator Facility (JLab) to study the pion form factor from $Q^2 = 0.6$–1.6 GeV^2. Because of the excellent properties of the electron beam and experimental setup at JLab, L/T separated cross sections were determined with high accuracy. These data were used to determine the value of F_π and the results were published in Ref. [13]. Since then, the whole analysis chain has been repeated with careful investigation of all steps, including the contribution of various systematic uncertainties to the final uncertainty of the separated cross sections. Furthermore, the method to determine F_π from the longitudinal cross sections was reinvestigated, leading to a different method to extract F_π. In this article, we report on these studies and present final results for the longitudinal and transverse cross sections, as well as the extracted values of F_π from these data. We also discuss in detail the extraction of F_π from the measured cross sections, and the related extraction uncertainties (model dependence).

II. EXPERIMENT AND CROSS SECTION DATA ANALYSIS

The cross section for pion electroproduction can be written as

$$\frac{d^3\sigma}{dE'd\Omega_{e'}d\Omega_\pi} = \Gamma_V J(t) \frac{d^2\sigma}{dtd\phi}, \qquad (2)$$

where

$$\Gamma_v = \frac{\alpha}{2\pi^2} \frac{E'_e}{E_e} \frac{1}{Q^2} \frac{1}{1-\epsilon} \frac{W^2 - M^2}{2M} \qquad (3)$$

is the virtual photon flux factor, ϕ is the azimuthal angle of the outgoing pion with respect to the electron scattering plane,

$t = (p_\pi - q)^2$ is the Mandelstam variable, J is the Jacobian for the transformation from $d\Omega_\pi$ to $dtd\phi$, and W is the photon-nucleon invariant mass.

The twofold differential cross section can be written as

$$2\pi \frac{d^2\sigma}{dtd\phi} = \epsilon \frac{d\sigma_L}{dt} + \frac{d\sigma_T}{dt} + \sqrt{2\epsilon(\epsilon+1)} \frac{d\sigma_{LT}}{dt} \cos\phi$$
$$+ \epsilon \frac{d\sigma_{TT}}{dt} \cos 2\phi, \qquad (4)$$

where $\epsilon = (1 + 2\frac{|\mathbf{q}^2|}{Q^2} \tan^2 \frac{\theta}{2})^{-1}$ is the virtual-photon polarization parameter. The $\sigma_X \equiv \frac{d\sigma_X}{dt}$ cross sections depend on W, Q^2, and t. By using the ϕ acceptance of the experiment and taking data for the same (central) kinematics (W, Q^2, t) at two energies, and thus two values of ϵ, the cross sections σ_L, σ_T, σ_{LT}, and σ_{TT} can all be determined.

Using 2.4–4 GeV electron beams impinging on a liquid hydrogen target, data for the ^{1}H$(e, e'\pi^+)n$ reaction were taken at a central value of $W = 1.95$ GeV for central Q^2 values of 0.6, 0.75, 1.0, and 1.6 GeV^2. The scattered electron was detected in the short orbit spectrometer (SOS) and the produced pion in the high momentum spectrometer (HMS) of Hall C.

The data analysis is an updated version of that in Ref. [13]. First, experimental yields were determined. Electrons in the SOS were identified by using the combination of a lead glass calorimeter and gas Čerenkov detector. Pion identification in the HMS was accomplished by requiring no signal in a gas Čerenkov detector and by using time-of-flight between two scintillator hodoscope planes. The momenta of the scattered electron and the pion at the target vertex were reconstructed from the wire chamber information of the spectrometers, correcting for energy loss in the target. From these, the values of Q^2, W, t, and the missing mass were reconstructed. A cut on the latter of 0.925 to 0.96 GeV was used to select the neutron exclusive final state, excluding additional pion production (Fig. 1). Experimental yields as function of Q^2, W, t, and ϕ were then determined by subtracting random coincidences (varying with bin but typically 1.2%) and aluminum target window contributions (typically 0.6%) and correcting for trigger, tracking and particle-identification efficiencies, pion absorption, local target-density reduction due to beam heating, and dead times. Details of these procedures are similar to those found in Ref. [14].
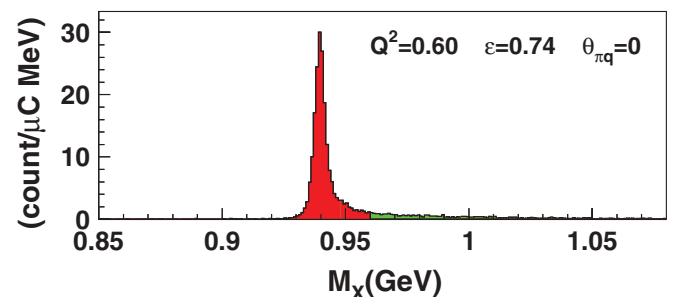

FIG. 1. (Color online) Representative missing mass distribution. Cuts at 0.925 and 0.960 GeV were applied to select the recoil neutron final state.

Cross sections were obtained from the yields using a detailed Monte Carlo (MC) simulation of the experiment, which included the magnets, apertures, detector geometries, realistic wire chamber resolutions, multiple scattering in all materials, optical matrix elements to reconstruct the particle momenta at the target from the information of the wire chambers of the spectrometers, pion decay (including misidentification of the decay muon as a pion), and internal and external radiative processes.

Calibrations with the overdetermined ^{1}H$(e, e'p)$ reaction were instrumental in various applications. The beam momentum and the spectrometer central momenta were determined absolutely to better than 0.1%, whereas the incident beam angle and spectrometer central angles were determined with an absolute accuracy of about 0.5 mrad. The spectrometer acceptances were checked by comparison of the data to the MC simulations. Finally, the overall absolute cross section normalization was checked. The calculated yields for $e + p$ elastics agreed to better than 2% with predictions based on a parametrization of the world data [15].

In the pion production reaction, the experimental acceptances in W, Q^2, and t are correlated. By using a realistic cross-section model in the MC simulation, possible errors resulting from averaging the measured yields when calculating cross sections at average values of W, Q^2, and t can be minimized. A phenomenological cross-section model was obtained (see below) by fitting the different cross sections σ_X of Eq. (4) globally to the data as a function of Q^2 and t in the whole range of Q^2. The dependence of the cross section on W was assumed to follow the phase-space factor $(W^2 - M_p^2)^{-2}$, which is supported by previous data [12].

The experimental cross sections can then be calculated from the measured and simulated yields via the relation

$$\left[\frac{d\sigma(\overline{W}, \overline{Q}^2, t, \phi)}{dt} \right]_{\exp} = \frac{\langle Y_{\exp} \rangle}{\langle Y_{\mathrm{MC}} \rangle} \left[\frac{d\sigma(\overline{W}, \overline{Q}^2, t, \phi)}{dt} \right]_{\mathrm{MC}}. \quad (5)$$

This was done for five bins in t at each of the four Q^2 values. Here, $\langle Y \rangle$ indicates that the yields were averaged over the W and Q^2 acceptance, $\overline{W}$ and $\overline{Q}^2$ being the acceptance (of high and low ϵ together) weighted average values for that t bin. By using these average values, possible errors due to extrapolating the MC model cross section used to outside the region of the experimental data, is avoided.

By combining for every t bin (and for the four values of Q^2) the ϕ-dependent cross sections measured at two values of the incoming electron energy, and thus of ϵ, the experimental values of σ_L, σ_T, σ_{LT}, and σ_{TT} can be determined by fitting the ϕ and ϵ dependence (Fig. 2). In this fit, the leading order $\sin \theta$ ($\sin^2 \theta$) of σ_{LT} (σ_{TT}), where θ is the angle between the three-momentum transfer and the direction of the outgoing pion, was taken into account.[1] Those values were then used to improve on the model cross section used in the MC simulation. This
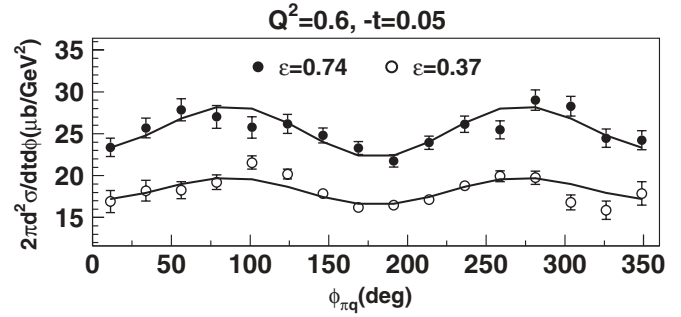
FIG. 2. Example of the measured cross sections, $d^2\sigma/dt d\phi$, as a function of ϕ at $Q^2 = 0.6$ GeV^2 for two values of ϵ. The curves shown represent the model cross section used in the Monte Carlo simulation.

whole procedure was iterated until the values of σ_L, σ_T, σ_{LT}, and σ_{TT} converged. The dependence of σ_L (and σ_T) on the MC input model was small (see below).

The separated cross sections σ_L and σ_T are shown in Fig. 3. They are presented as differential cross sections $d\sigma/dt$ as a function of t at the center of the t bin. The longitudinal cross section exhibits the expected t-pole behavior. The transverse cross section is mostly flat.

The total uncertainty in the experimental cross sections is a combination of statistical and systematic uncertainties. All contributions to the systematic uncertainty were carefully investigated, also using the results of extensive single-arm L/T separation experiments and of ^{1}H$(e, e'p)$ calibration reactions in Hall C [16]. The experimental systematic uncertainties include contributions that, like the statistical uncertainties, are uncorrelated between the measurements at the two ϵ values and others that are correlated. Most of the uncorrelated ones are common to all t bins, but there is a small contribution, estimated as 0.7%, that is also uncorrelated in t. The ϵ-uncorrelated uncertainties in σ_L are inflated by the factor $1/\Delta\epsilon$ in the L/T separation, where $\Delta\epsilon$ is the difference (typically 0.3) in the photon polarization between the two measurements. The effect on σ_T depends on the exact ϵ values. The ϵ-uncorrelated systematic uncertainty in the unseparated cross sections common for all t bins was estimated to be 1.7%, whereas the total correlated uncertainty is 2.8–4.1%, depending on t. Apart from a dependence of the separated cross sections on the MC model used, which ranges from 0.2% to a maximum of 3% for one highest t bin, the largest contributions are: the detection volume (1.5%), dependence of the extracted cross sections on the momentum and angle calibration (1%), target density (1%), pion absorption (1.5%), pion decay (1%), the simulation of radiative processes (1.5%), and detector efficiency corrections (1%). The overall uncertainty is slightly smaller than used in Ref. [13].

The unseparated cross sections and hence also the values of σ_L and σ_T of the present analysis differ from those of our earlier analysis presented in Ref. [13]. Compared to that analysis, small adjustments were made in the values of cuts and

---

[1]In the previous analysis [13], first σ_{LT} and σ_{TT} were determined by adjusting their values (plus a constant term) until the ratios $Y_{\exp}/Y_{\mathrm{MC}}$ were constant as function of θ and ϕ. After that, σ_L and σ_T were determined in a Rosenbluth separation. The present method is more

straightforward and has the advantage that the uncertainties in the separated cross sections are obtained more directly.

TABLE I. Separated cross sections σ_L and σ_T from this work. The two listed uncertainties for σ_L are the combination of statistical and t-uncorrelated systematic uncertainties, and the combination of the ϵ-correlated and -uncorrelated uncertainties. The statistical and t-uncorrelated uncertainties are applied before fitting the VGL model to the data, whereas the ϵ-correlated and -uncorrelated uncertainties are applied afterwards. The listed errors for σ_T include all experimental uncertainties.

$\overline{Q^2}$ (GeV^2)	$\overline{W}$ (GeV)	$-t$ (GeV^2)	$d\sigma_L/dt$ (μb/GeV^2)	$d\sigma_T/dt$ (μb/GeV^2)
0.526	1.983	0.026	$31.360 \pm 1.602, 1.927$	8.672 ± 1.241
0.576	1.956	0.038	$24.410 \pm 1.119, 1.774$	10.660 ± 1.081
0.612	1.942	0.050	$20.240 \pm 1.044, 1.583$	10.520 ± 1.000
0.631	1.934	0.062	$14.870 \pm 1.155, 1.366$	10.820 ± 0.992
0.646	1.929	0.074	$11.230 \pm 1.469, 1.210$	10.770 ± 1.097
0.660	1.992	0.037	$20.600 \pm 1.976, 1.895$	9.812 ± 1.532
0.707	1.961	0.051	$16.280 \pm 1.509, 1.788$	10.440 ± 1.344
0.753	1.943	0.065	$14.990 \pm 1.270, 1.573$	8.580 ± 1.150
0.781	1.930	0.079	$11.170 \pm 1.214, 1.416$	9.084 ± 1.091
0.794	1.926	0.093	$9.949 \pm 1.376, 1.277$	8.267 ± 1.110
0.877	1.999	0.060	$14.280 \pm 1.157, 1.103$	7.084 ± 0.791
0.945	1.970	0.080	$11.840 \pm 0.887, 0.978$	6.526 ± 0.657
1.010	1.943	0.100	$9.732 \pm 0.773, 0.837$	5.656 ± 0.572
1.050	1.926	0.120	$7.116 \pm 0.789, 0.747$	5.926 ± 0.570
1.067	1.921	0.140	$4.207 \pm 1.012, 0.612$	5.802 ± 0.656
1.455	2.001	0.135	$5.618 \pm 0.431, 0.442$	3.613 ± 0.294
1.532	1.975	0.165	$4.378 \pm 0.356, 0.390$	3.507 ± 0.257
1.610	1.944	0.195	$3.191 \pm 0.322, 0.351$	3.528 ± 0.241
1.664	1.924	0.225	$2.357 \pm 0.313, 0.310$	3.354 ± 0.228
1.702	1.911	0.255	$2.563 \pm 0.356, 0.268$	2.542 ± 0.227

efficiencies. Also, a small mistake was found in calculating the value of θ, which affects the calculation of the cross section in Eq. (5). Finally, as mentioned, the method to separate the cross sections was changed. The cross sections in Table I are our final values. Except for a few cases, the difference with the previous values is well within the total uncertainty quoted in Ref. [13]. As an example, the old and the new cross sections for the case $Q^2 = 0.75$ GeV^2 are shown in Fig. 4. It can be seen that the differences in the extracted unseparated cross sections (top panels) are very small, but the L/T separation increases them. On average over the four Q^2 cases, σ_L is 6% smaller than in Ref. [13] and σ_T is 3% larger. The largest differences occur for $Q^2 = 1.0$ GeV^2, where σ_L is 14% smaller and σ_T is 10% larger.

III. EXTRACTION OF $F_\pi(Q^2)$ FROM THE DATA

It should be clear that the differential cross sections σ_L versus t over some range of Q^2 and W are the actual observables measured by the experiment. The extraction of the pion form factor from these cross sections can be done in a number of approaches, each with their own merits and associated uncertainties.

Frazer [17] originally proposed that F_π be extracted from σ_L via a kinematic extrapolation to the pion pole, and that this be done in an analytical manner, à la Chew-Low [18]. This extrapolation procedure fails to produce a reliable

answer, because different polynomial fits, each of which are equally likely in the physical region, differ considerably when continued to $t = m_\pi^2$. Some attempts were made [19] to reduce this uncertainty by providing some theoretical constraints on the behavior of the pion form factor in the unphysical region, but none proved adequate.

Bebek *et al.* [10] embraced the use of theoretical input when they used the Born term model of Berends [20] to perform a form-factor determination. Brauel *et al.* [12] similarly used the Born term model of Gutbrod and Kramer [21] to extract F_π. The presence of the nucleon and its structure complicates the theoretical model used, and so an unavoidable implication of this method is that the extraction of the pion form factor becomes model dependent.

As in Ref. [13,22], the Regge model by Vanderhaeghen, Guidal, and Laget (VGL, Ref. [23]) is used here to extract F_π. In this model, the polelike propagators of Born term models are replaced with Regge propagators, and so the interaction is effectively described by the exchange of a family of particles with the same quantum numbers instead of the exchange of one particle. The model was first applied to pion photoproduction. Most of the model's free parameters were determined from data on nucleon resonances. The use of Regge propagators, and the fact that both the π ($J = 0$) and the ρ ($J = 1$) trajectories are incorporated in the model proved to be essential to obtain a good description of the W and t dependence of the photoproduction data for both π^+ and π^- particles. For electroproduction, the pion form factor and the $\rho\pi\gamma$ form
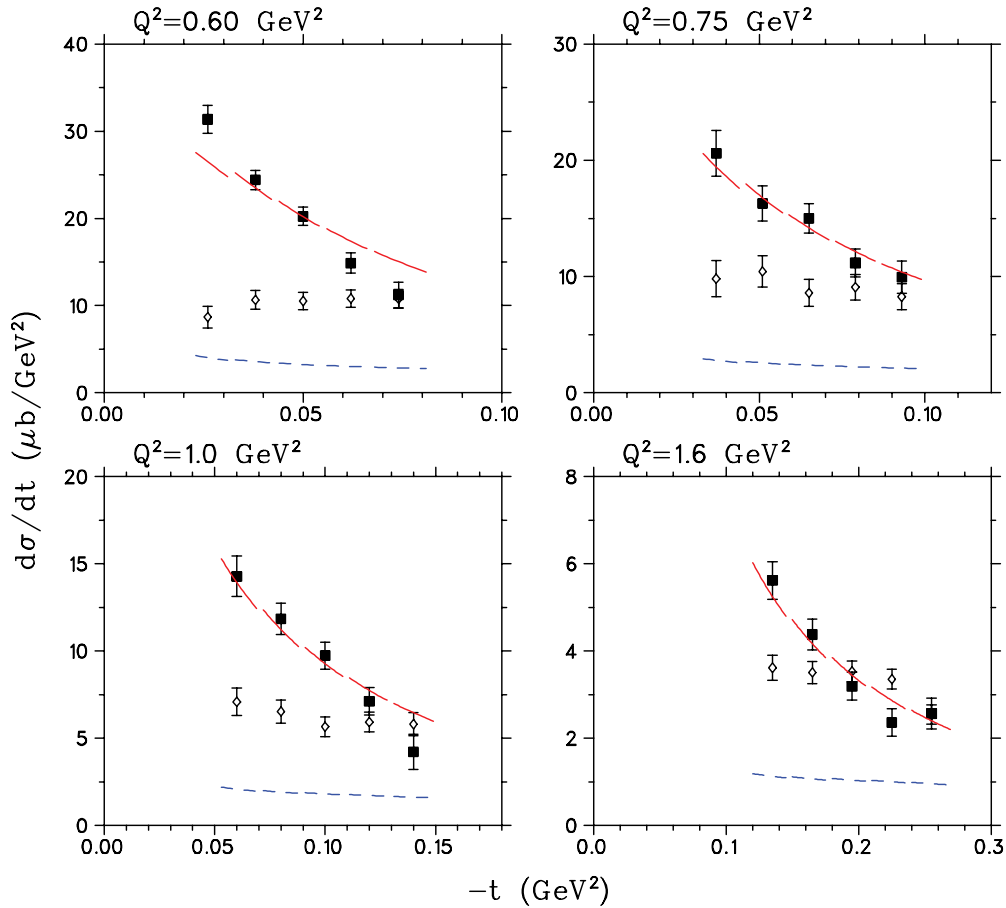
FIG. 3. (Color online) Separated cross sections σ_L (solid) and σ_T (open). The error bars represent the combination of statistical and t uncorrelated systematic uncertainties. In addition, there is an overall systematic uncertainty of about 6%, mainly from the t correlated, ϵ uncorrelated systematic uncertainty. The solid and dashed curves denote VGL model calculations for σ_L and σ_T with parameters $\Lambda_\pi^2 = 0.393$, 0.373, 0.412, 0.458 GeV^2 for $Q^2 = 0.6$–1.6 GeV^2, and with common $\Lambda_\rho^2 = 1.5$ GeV^2. The discontinuities in the curves result from the different average $\overline{W}$ and $\overline{Q}^2$ of each t bin.

factor are added as adjustable parameters, parametrized with a monopole form

$$F_\pi(Q^2) = \left[1 + Q^2/\Lambda_\pi^2\right]^{-1}. \qquad (6)$$

The Regge model does a superior job of describing the t dependence of the differential pion electroproduction cross sections of Refs. [11,12] than the Born term model. Over the range of $-t$ covered by this work, σ_L is completely determined by the π trajectory, whereas σ_T is also sensitive to the ρ exchange contribution. The value of Λ_ρ^2 is poorly known, whereas Λ_π^2 is much better known and in the end is determined by the fitting of the model to the σ_L data.

The VGL model for certain choices of Λ_π^2 and Λ_ρ^2 is compared to our data in Fig. 3. The VGL cross sections have been evaluated at the same $\overline{W}$ and $\overline{Q}^2$ values as the data, resulting in the discontinuities shown. The model strongly underestimates σ_T for any value of Λ_ρ^2 used (variation of Λ_ρ^2 within reasonable values can change σ_T by up to 40%). Because the JLab data have been taken at relatively low values of $W \approx 1.95$ GeV, this may be due to contributions

from resonances, enhancing the strength in σ_T. No such terms are included explicitly in the Regge model. The VGL model calculation for σ_L gives the right magnitude, but the t dependence of the data is somewhat steeper than that of the calculations. This is most visible at $Q^2 = 0.6$ GeV^2. As in the case of σ_T, the discrepancy between the data and VGL is attributed to resonance contributions. This is supported by the fact that the discrepancy is strongest at the lowest Q^2 value, at higher Q^2 the resonance form factor reduces such contributions.

Given this discrepancy in shape between the VGL calculations and the σ_L data, the questions are as follows: (i) how to determine the value of F_π from the measured longitudinal cross sections σ_L and (ii) what is the associated "model uncertainty" in doing so? The difficulty is that there is no theoretical guidance for the assumed interfering background. This applies even if one assumes that the background is due to resonances: virtually nothing is known about the L/T character of resonances at $W = 1.95$ GeV, let alone their influence on σ_L (via interference with the VGL amplitude).
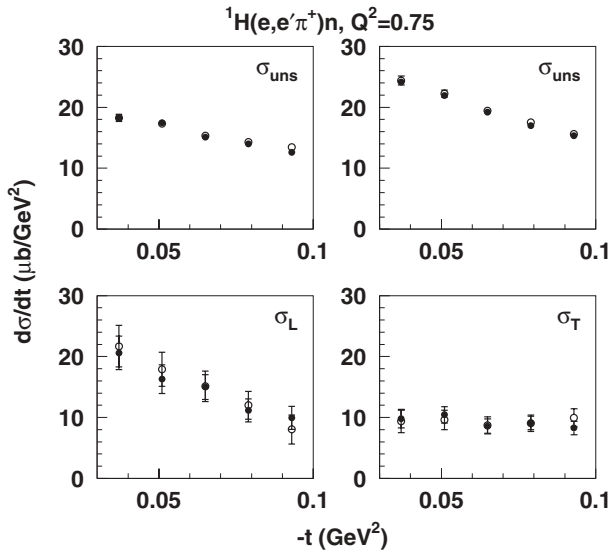
FIG. 4. Differential cross section comparison between our earlier $Q^2 = 0.75$ GeV^2 results (open circles) (Ref. [13]) and this work (filled circles). The unseparated cross sections ($\sigma_{uns} = \epsilon \sigma_L + \sigma_T$) at high and low ϵ are nearly identical, but the differences between the separated σ_L and σ_T are somewhat larger. The σ_{uns} error bars include the statistical and epsilon uncorrelated systematics only and are in many cases smaller than the plotting symbols. Those for $\sigma_{L,T}$ include the contribution of all statistical and systematic uncertainties.

A. Summary of our previous extraction method

In our previous analysis [13], the following procedure was adopted. When fitting the value of Λ_π^2 (and hence F_π) for the separate t bins the value of Λ_π^2 increases when $-t$ decreases, because the data are steeper in $|t|$ than the VGL calculations. The value of F_π extracted from the lowest $|t|$ bin, which is closest to the pole, was thus taken as a lower limit.

An upper limit for F_π was obtained by assuming that the background effectively yields a constant negative contribution to σ_L. This background and the value of Λ_π^2 were then fitted together, assuming that the background is constant with t. The fitted contribution of the background was found to drop strongly as Q^2 increased from 0.6 to 1.6 GeV^2. Because in σ_T this "missing background" (i.e., the difference between the data and VGL model) decreases, at least for $Q^2 = 0.6$ GeV^2, with decreasing $-t$ (Fig. 3), and assuming that this also holds for σ_L, these assumptions give an upper estimate for F_π. The best estimate for F_π was then taken as the average of the two results and one half of the average of the (relative) differences was taken as the "model uncertainty."

However, the asumptions made in this procedure may be questioned. First, the value of F_π extracted from the lowest $|t|$ bin does not have to be a lower limit and, second, the assumption of a negative interfering t-independent cross section in the upper limit calculation requires a special magnitude and phase for the interfering amplitude with respect to the VGL amplitude.

B. Another form factor extraction method

Since the publication of those results, we have looked at the discrepancy between the t dependence predicted by the

VGL model and the data in more detail by assuming, in addition to the VGL amplitude, a t-independent interfering background *amplitude*, and fitting the latter together with the value of Λ_π^2. The fitting uncertainty in Λ_π^2 varies between 5 and 18%, whereas the magnitude and phase of the fit background amplitude are very poorly constrained (uncertainties in the hundreds of percent).

Although the fitting uncertainties are very large, the results of this exercise suggest an interfering amplitude whose magnitude decreases monotonically with increasing Q^2, but whose phase with respect to the VGL amplitude does not necessarily result in a net-negative cross section contribution to σ_L, as has been assumed in the previous analysis. However, here also a special assumption was used, i.e., an interfering amplitude with a magnitude and phase that do not depend on t. Thus, determining F_π in this way is not a viable method, either.

C. Adopted form factor extraction method

Given that no information is available on the background, we are forced to make some assumptions in extracting F_π from these data. Our guiding principle is to minimize these assumptions to the greatest extent possible. The form-factor extraction method that we have adopted relies on the single assumption that the contribution of the background is smallest at the kinematic endpoint t_{min}.

Our best estimate for F_π is thus determined in the following manner. Using the value of Λ_π^2 as a free parameter, the VGL model was fitted to each t bin separately, yielding $\Lambda_\pi^2(\overline{Q^2}, \overline{W}, t)$ values as shown in Fig. 5. The values of Λ_π^2 tend to decrease as $-t$ increases, presumably because of an interfering background not included in the model. Because the pole cross section containing F_π increases strongly with decreasing $-t$, and the background presumably remains approximately constant, as suggested by the difference between data and VGL calculations for σ_T, we assume that the effect of this background will be smallest at the smallest value of $|t|$ allowed by the experimental kinematics, $|t_{min}|$. Thus, an extrapolation of Λ_π^2 to this physical limit is used to obtain our best estimate of F_π. The value of Λ_π^2 at t_{min} is obtained by a linear fit to the data in Fig. 5. The resulting Λ_π^2 and F_π values are listed in Table II. The first uncertainty given represents both the experimental and the linear fit extrapolation uncertainties.

TABLE II. Λ_π^2 and F_π values from this work, and the reanalyzed data from Ref. [12] using the same method. The first error includes all experimental and analysis uncertainties, and the second error is the "model uncertainty" as described in the text.

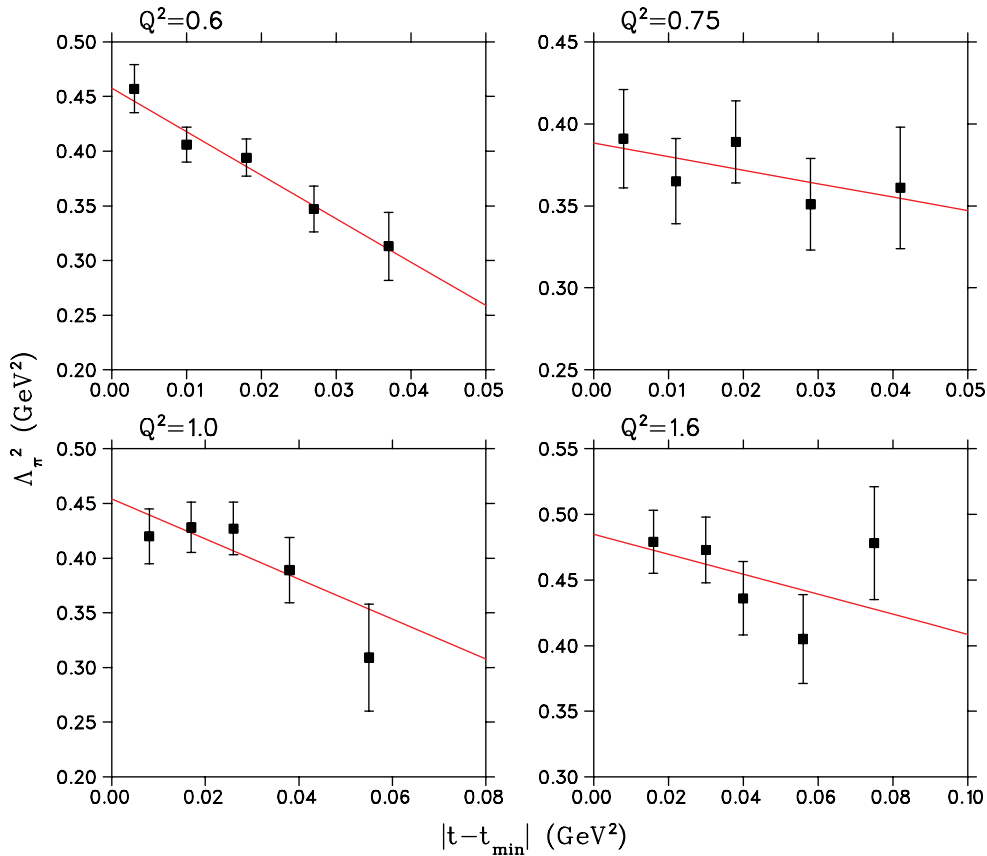| Q^2 (GeV^2)	W (GeV)	Λ_π^2 (GeV^2)	F_π
0.60	1.95	$0.458 \pm 0.031^{+0.255}_{-0.068}$	$0.433 \pm 0.017^{+0.137}_{-0.036}$
0.75	1.95	$0.388 \pm 0.038^{+0.135}_{-0.053}$	$0.341 \pm 0.022^{+0.078}_{-0.019}$
1.00	1.95	$0.454 \pm 0.034^{+0.075}_{-0.040}$	$0.312 \pm 0.016^{+0.035}_{-0.019}$
1.60	1.95	$0.485 \pm 0.038^{+0.035}_{-0.027}$	$0.233 \pm 0.014^{+0.013}_{-0.010}$
0.70	2.19	$0.627 \pm 0.058^{+0.096}_{-0.085}$	$0.473 \pm 0.023^{+0.038}_{-0.034}$

FIG. 5. (Color online) Values of Λ_π^2 determined from the fit of the VGL model to each t bin, and linear fit to same. The error bars reflect the statistical and t-uncorrelated systematic uncertainties. The additional overall systematic uncertainties, which are applied after the fit, are not shown.

The F_π values listed in Table II correspond to the true values within the context of the VGL model if, and only if, the background vanishes at $|t - t_{\min}| = 0$. Because of the uncertainty inherent in this assumption, we also estimate a "model uncertainty" to account for the possible influence of the missing ingredient in the VGL model (background) at $|t - t_{\min}| = 0$. Lacking a model for the background, we can only try to make a fair estimate of this uncertainty. This was done by looking at the variation in the fitted values of Λ_π^2 when using two different assumptions for the background. We used the two cases considered earlier in this article when trying to determine F_π. The first case assumes the t-independent negative background in addition to the VGL model used in Sec. III A. The second case assumes the interfering background amplitude with a t-independent magnitude and phase discussed in Sec. III B. However, here they are not used to determine F_π, but only to estimate the model uncertainty in our best value of F_π determined above.

The estimated model uncertainty is determined from the spread of the Λ_π^2 values at each Q^2 given by these two methods. Each effectively represents a different background interference with the VGL model. To keep the number of degrees of freedom the same in all cases, the background was fixed to the minimum χ^2 value determined in each of the above two studies, and Λ_π^2 and its uncertainty was then determined in a one-parameter fit of the VGL model plus background to the σ_L

data. Because there is a strong statistical overlap between the two fits, the statistical plus random uncertainties of the data were quadratically removed from the Λ_π^2 uncertainties. The model uncertainty at each Q^2 is then assigned to be the range plus fitting uncertainty given by the two methods, relative to the value of Λ_π^2 at $t_{\min}$. The resulting (asymmetric) uncertainties are listed as the second uncertainty in Table II.

The model uncertainty in the F_π value drops from about 20% at $Q^2 = 0.6$ GeV^2 to about 5% at 1.6 GeV^2. This is consistent with the fact that the discrepancy with the t dependence of the VGL calculation is smaller for the larger values of Q^2. It is also at least compatible with the idea that resonance contributions, which presumably have a form factor that drops fast with Q^2, are responsible. The corresponding model uncertainty quoted in Ref. [13] was approximately 8.5% at all Q^2, but that was based on a more restrictive assumption on the background (in essence case 1).

IV. RESULTS AND DISCUSSION

Because of the arguments given above, the values presented in Table II and Fig. 6 are our final estimate of F_π from these data using this model. However, we stress that the primordial results of our experiment are the σ_L cross sections. When improved models for the ^{1}H($e, e'\pi^+$)n reaction become
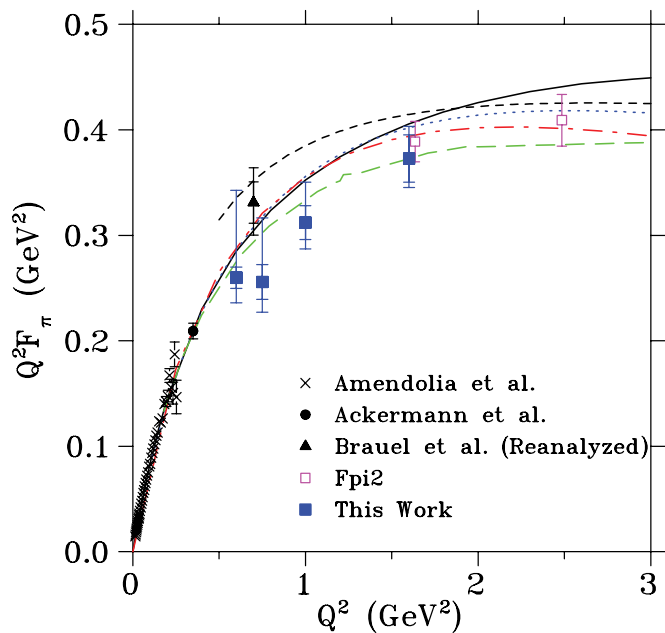
FIG. 6. (Color online) $Q^2 F_\pi$ data from this work, compared to previously published data. The Brauel *et al.* [12] point has been reanalyzed using the F_π extraction method of this work. The outer error bars for this work and the reanalyzed Brauel *et al.* data include all experimental and model uncertainties, added in quadrature, whereas the inner error bars reflect the experimental uncertainties only. Also shown are the light front quark model [6] (dash-dot), Dyson-Schwinger [7] (solid), QCD sum-rule [24] (dot), dispersion relation [25] (long-dash), and quark-hadron duality [26] (short-dash) calculations.

available, other (better) values of F_π may be extracted from the same cross sections.

The present values for F_π are between 7 and 16% smaller than our previously published values [13], which is about the combined experimental and model uncertainty. The largest difference is at $Q^2 = 0.75$ GeV^2. On average, one-quarter of the difference is because the final values of σ_L are smaller than those of Ref. [13] (see Fig. 4 for a representative comparison), and the remaining three-quarters are due to the F_π extraction method, the present method being closer to the method used in Ref. [13] to obtain the lower limit.

Analyses of other data at higher W indicate that the discrepancy with the t dependence of the VGL calculation is much smaller at higher values of W. The data from Brauel *et al.* [12], taken at $Q^2 = 0.70$ GeV^2 and a value of $W = 2.19$ GeV, were reanalyzed using the F_π extraction method presented here. The result is 0.4% higher than that obtained using the F_π extraction method of Ref. [13]. This indicates that our F_π extraction methods are robust when the background contribution is small, as appears to be the case at this higher value of W.

The data from our second experiment [22] at $W = 2.22$ GeV and $Q^2 = 1.6, 2.45$ GeV^2 are also shown in Fig. 6. There, the VGL model adequately describes the t dependence of the σ_L data, again indicating that the background contributions for σ_L are smaller at higher W, even though the model strongly underpredicts the magnitude of σ_T. In that case, the

VGL model was fit to the full t range of the σ_L data with only small fitting uncertainties. It is seen in the figure that the revised $Q^2 = 1.6$ GeV^2 result from this work agrees well with that from our second experiment, taken at higher W and 30% closer to the π^+ pole. The excellent agreement between these two results, despite their significantly different $t_{\min}$ values, indicates that the uncertainties due to the π^+ electroproduction reaction mechanism seem to be under control, at least in this Q^2 range.

Figure 6 compares our final data from this work and from our second experiment [22] to several QCD-based calculations. The combined data sets are consistent with a variety of models. Up to $Q^2 = 1.5$ GeV^2, the Dyson-Schwinger calculation of Ref. [7], the light front quark model calculation of Ref. [6], and the QCD sum-rule calculation of Ref. [24] are nearly identical, and are all very close to the monopole form factor constrained by the measured pion charge radius [9]. Such a form factor reflects non-perturbative physics. Our revised data are below the monopole curve. A significant deviation would indicate the increased role of perturbative components at moderate Q^2, which provide in that region a value of $Q^2 F_\pi \approx 0.15$–0.20 only [2]. The dispersion relation calculation of Geshkenbein *et al.* [25] is closer to our results in the $Q^2 = 0.6$–1.6 GeV^2 region, whereas still describing the low Q^2 data used for determining the pion charge radius. The quark-hadron duality calculation by Melnitchouk [26] is not expected to be valid below $Q^2 = 2.0$ GeV^2. This is reflected in its significant deviation from the monopole curve at low Q^2. To better distinguish between these different models, it is clear that especially higher Q^2 data, as well as more data at higher values of W in the $Q^2 = 0.6$–1.6 GeV^2 region, are needed. Plans are underway to address both of these at JLab.

V. SUMMARY AND CONCLUSIONS

To summarize, the data analysis for our ^{1}H$(e, e'\pi^+)n$ experiment at $Q^2 = 0.6$–1.6 GeV^2, centered at $W = 1.95$ GeV, has been repeated with careful inspection of all steps. The final unseparated cross sections presented here are in most cases consistent with our previous analysis within experimental uncertainties. After the magnifying effect of the L/T separation, the resulting σ_T values are slightly larger than before, and the σ_L values are correspondingly smaller. The experimental systematic uncertainties were critically reviewed, and are slightly smaller compared to the previous analysis.

As before, we use a fit of the Regge model of Ref. [23] to our σ_L data to extract F_π. The data display a steeper t dependence than the model, which we attribute to the presence of longitudinal background contributions not included in the model. After revisiting our prior assumptions used to extract F_π from σ_L with the model, we conclude that some of our prior analysis assumptions were unwarranted. Therefore, we employ a revised F_π extraction method which relies only on the assumption that the background contributions are minimal at $t_{\min}$. The resulting values are our best estimate of F_π from these data with this model, and are between 8 and 16% smaller than before, primarily due to the different extraction method.

The Brauel *et al.* [12] data at similar Q^2 but higher W are robust against our fitting assumptions, consistent with our expectation that a longitudinal background contribution not included in the Regge model is the cause of the discrepancy.

The new analysis, in addition to providing our final F_π results for the $Q^2 = 0.6$–1.6 GeV^2 range, gives an indication of the contribution of the analysis assumptions to the F_π determination. A detailed analysis yields model uncertainties that decrease with increasing Q^2 and W. They are consistent with the differences in the values of F_π determined using the previous and present extraction methods. They indicate that, given the present electroproduction model, the uncertainty in the determination of F_π in this W and Q^2 range is of the order of 10%.

The revised data indicate that for $Q^2 > 0.5$ GeV^2, F_π starts to fall below the monopole curve that describes the low Q^2 elastic-scattering data. These results are consistent with those of our second, more precise experiment at higher Q^2 and W

[22]. The two sets of data at $Q^2 = 1.6$ GeV^2 are taken with significantly different t_{min}, and so if the various form factor extraction issues were not being handled well by the VGL model, a significant discrepancy would have been expected to result. Their good agreement lends further credibility to the analysis presented here. It will be useful to acquire additional electroproduction data in the $0.5 < Q^2 < 1.5$ GeV^2 range at higher W to be able to extract more precise values of F_π without the difficulties encountered here.

ACKNOWLEDGMENTS

[1] G. P. Lepage and S. J. Brodsky, Phys. Lett. **B87**, 359 (1979).

[2] A. P. Bakulev, K. Passek-Kumericki, W. Schroers, and N. G. Stefanis, Phys. Rev. D **70**, 033014 (2004).

[3] B. Melic, B. Nizic, and K. Passek, Phys. Rev. D **60**, 074004 (1999).

[4] A. V. Radyushkin, Nucl. Phys. **A532**, 141c (1991).

[5] V. M. Braun, A. Khodjamirian, and M. Maul, Phys. Rev. D **61**, 073004 (2000).

[6] C.-W. Hwang, Phys. Rev. D **64**, 034011 (2001).

[7] P. Maris and P. C. Tandy, Phys. Rev. C **62**, 055204 (2000).

[8] G. Sterman and P. Stoler, Annu. Rev. Nucl. Part. Sci. **47**, 183 (1997).

[9] S. R. Amendolia *et al.*, Nucl. Phys. **B277**, 168 (1986).

[10] C. J. Bebek *et al.*, Phys. Rev. D **17**, 1693 (1978).

[11] H. Ackermann *et al.*, Nucl. Phys. **B137**, 294 (1978).

[12] P. Brauel *et al.*, Z. Phys. C **3**, 101 (1979).

[13] J. Volmer *et al.*, Phys. Rev. Lett. **86**, 1713 (2001).

[14] J. Volmer, Ph.D. thesis, Vrije Universiteit, Amsterdam (2000).

[15] P. E. Bosted, Phys. Rev. C **51**, 409 (1995).

[16] M. E. Christy *et al.*, Phys. Rev. C **70**, 015206 (2004).

[17] W. R. Frazer, Phys. Rev. **115**, 1763 (1959).

[18] G. F. Chew and F. E. Low, Phys. Rev. **113**, 1640 (1959).

[19] B. H. Kellett and C. Verzegnassi, Nuovo Cimento A **20**, 194 (1974).

[20] F. A. Berends, Phys. Rev. D **1**, 2590 (1970).

[21] F. Gutbrod and G. Kramer, Nucl. Phys. **B49**, 461 (1972).

[22] T. Horn *et al.*, Phys. Rev. Lett. **97**, 192001 (2006).

[23] M. Vanderhaeghen, M. Guidal, and J.-M. Laget, Phys. Rev. C **57**, 1454 (1998); Nucl. Phys. **A627**, 645 (1997).

[24] V. A. Nesterenko and A. V. Radyushkin, Phys. Lett. **B115**, 410 (1982).

[25] B. V. Geshkenbein, Phys. Rev. D **61**, 033009 (2000).

[26] W. Melnitchouk (private communication, 2006), and Eur. Phys. J. A **17**, 233 (2003).